Available online at www.sciencedirect.com
ScienceDirect
Trans. Nonferrous Met. Soc. China 24(2014) 3894−3900
Transactions of Nonferrous Metals Society of China
www.tnmsc.cn

Preparation and wear properties of TiB_2/Al−30Si composites via in-situ melt reactions under high-energy ultrasonic field

Song-li ZHANG[1], Xian-wei DONG[2], Yu-tao ZHAO[1], Man-ping LIU[1], Gang CHEN[1], Zhen-kun ZHANG[1], Yu-ying ZHANG[1], Xue-hua GAO[1]

1. School of Materials Science and Engineering, Jiangsu University, Zhenjiang 212013, China;
2. School of Mining Engineering, Hebei United University, Tangshan 063009, China

Received 17 October 2013; accepted 16 November 2014

Abstract: TiB_2/Al−30Si composites were fabricated via in-situ melt reaction under high-energy ultrasonic field. The microstructure and wear properties of the composite were investigated by XRD, SEM and dry sliding testing. The results indicate that TiB_2 reinforcement particles are uniformly distributed in the aluminum matrix under high-energy ultrasonic field. The morphology of the TiB_2 particles is in circle-shape or quadrangle-shape, and the size of the particles is 0.1−1.5 μm. The primary silicon particles are in quadrangle-shape and the average size of them is about 10 μm. Hardness values of the Al−30Si matrix alloy and the TiB_2/Al−30Si composites considerably increase as the high energy ultrasonic power increases. In particular, the maximum hardness value of the in-situ composites is about 1.3 times as high as that of the matrix alloy when the ultrasonic power is 1.2 kW, reaching 412 MPa. Meanwhile, the wear resistance of the in-situ TiB_2/Al−30Si composites prepared under high-energy ultrasonic field is obviously improved and is insensitive to the applied loads of the dry sliding testing.
Key words: TiB_2/Al−30Si composite; in-situ melt reaction; high-energy ultrasonic field; wear properties

1 Introduction

Al−Si alloys are widely used in traffic tools, aerospace industries and electronic products areas due to their high wear resistance, excellent castability, high specific strength, strong heat conductive ability and low thermal expansion coefficient [1−3]. However, with increasing silicon content, the massive polygonal primary silicon and long needle-like eutectic silicon in hypereutectic Al−Si alloys split the matrix, which leads to the decrease of plasticity and toughness and limits further improvement of the properties of hypereutectic Al–Si alloys and the applications in wearing parts. In order to improve the hypereutectic Al−Si alloys' integrated properties, various processing technologies have been tried. Some of them are micro-alloying element modifying treatment such as Na, Sr, P [4−6], new processing techniques such as rheocasting, rapid solidification, spray forming, equal channel angular pressing (ECAP), and ceramics particle (fiber) composite technologies such as ex-situ SiC_p, Al_2O_{3p}, and the above technology combinations [7−12]. Among all the synthesis technologies of the composite, the in-situ melt reaction technology is one of the most promising methods. The ceramic-reinforced aluminum−silicon matrix composites by in-situ melt reaction synthesis show special merits as follows: 1) the thermodynamics stability of the in-situ reinforced particles is better than that of the ex-situ reinforcement particles; 2) the interface between in-situ particles and metal matrix is neat due to the fact that in-situ particles are formed in metal matrix, and the interface bonding intensity is high; 3) the size of the in-situ particles is fine and the distribution in metal matrix is uniform; 4) the metal melt can directly be moulded into parts with complicated shape and size; 5) the equipment and process are simple and the reinforcement particles are not needed for

Foundation item: Project (51174098) supported by the National Natural Science Foundation of China; Project (kjsmcx0903) supported by the Foundation of the Jiangsu Province Key Laboratory of Materials Tribology, China; Project (1202015B) supported by the Postdoctoral Science Foundation of Jiangsu Province, China; Project (03) supported by the Undergraduate Practice-Innovation Training Foundation of Jiangsu University, China; Projects (GY2012020, GY2013032) supported by the Science and Technology Support Plan Project Foundation of Zhenjiang City, China
Corresponding author: Yu-tao ZHAO; Tel: +86-511-88797658; E-mail: zhaoyt@ujs.edu.cn
DOI: 10.1016/S1003-6326(14)63548-2

pre-process, and thus the cost is low.

Although outstanding progress has been made in in-situ aluminum matrix composites in recent years, the microstructural and mechanical characteristics of the in-situ composites have not been yet fully understood. In particular, the ultrasonic technology is rarely used in the fabrication of the composites. SUSLICK [13] suggested that ultrasonic waves can generate small cavities in melt that can affect the chemical reaction dynamics. YANG et al [14] successfully fabricated bulk A356 composites reinforced with uniform dispersion of nano-sized SiC particles by an ultrasonic-assisted casting method. However, the combinations of both the in-situ and the ultrasonic technologies, have not been reported in the fabrication of the aluminum matrix composites.

In this work, the in-situ TiB_2 particle reinforced Al−30Si alloy matrix composites were fabricated under high-energy ultrasonic field, and the microstructures and wear properties of the as-prepared composites were comparatively investigated with those of the Al−30Si matrix alloy and the composites prepared without and with the ultrasonic field. In addition, the effects of the high-energy ultrasonic field on the size and morphology of the particles in the composites were discussed.

2 Experimental

The raw materials are Al−30Si ingots, inorganic salt K_2TiF_6 and KBF_4 powders (average size of 20 μm). Firstly, the inorganic salt K_2TiF_6 and KBF_4 powders were dehydrated at 250 °C for 3 h in an electric furnace. The Al−30Si alloy ingots were heated at 5 °C/min in graphite crucible (100 mm×120 mm×240 mm) in an electric furnace under nitrogen gas protection. When the temperature of the melt was 850 °C, the well mixed powders (mass ratio of K_2TiF_6 to KBF_4 was 1:1.3) with a mass ratio of 15% (to the total Al−30Si alloy melt) were added and pressed into the aluminum melt with a campanulate graphite mantle. The mantle was used to avoid the aluminum melt floating onto the surface. During the in-situ melt reactions, the ultrasonic generation system was turned on and the cylindrical amplitude lever was immersed into the aluminum about 5 mm in depth. Figure 1 shows the schematic illustration of the experimental setup. The frequency of the ultrasonic generator was 20 kHz and the maximum ultrasonic power of the equipment was 2.0 kW. The cylindrical amplitude lever with the diameter of 10 mm was made of a titanium alloy. To avoid the titanium alloy doping into the aluminum molten, a resistant high-temperature covering material was used to spray on the tip of the cylindrical amplitude lever of about 20 mm in length in axial direction and was dried. After 45 min, the melt was degassed, slag-removed and refined, and poured into a copper mould. After cooling to the room temperature in air, the composite ingot was processed as the testing specimens. The wear test specimens were sliced into discs with 30 mm in diameter and 8 mm in thickness by a linear cutting machine. The test surface of the composite specimen was polished using grade 1200 emery paper. The counter sliding pin of 40Cr steel was 5 mm in diameter and 20 mm in length. The roughness (R_a) of both the composite discs and the 40Cr steel pin was about 0.1 μm.

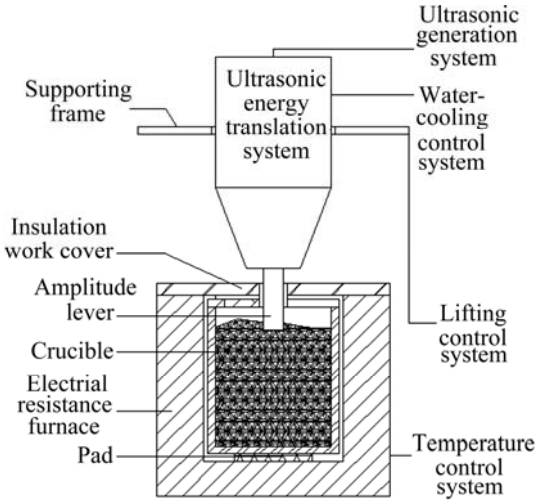

Fig. 1 Schematic illustration of experimental setup

An X-ray diffractometer (XRD, Dmax2500PC) using Cu K_α radiation was used to the determine the phase component of the as-prepared specimens, and scanning electron microscopy (SEM, JEOL, JSM-7001F) was used to analyze the microstructures. Wear property tests of the specimens were carried out at room temperature by using a wear apparatus (MG−2000) at a sliding velocity of 0.42 m/s. The diameter of the wear track was 23 mm. The wear mass loss of the specimens after cleaning in acetone was measured using an electron balance (MA110) with a sensitivity of 0.01 mg. The wear properties are the average values of three tests under each condition.

3 Results and discussion

3.1 Phase components of composites

Phase components of the prepared composites were determined by XRD analysis. The XRD pattern is shown in Fig. 2. As shown in the pattern, the Al, Si and TiB_2 phases are obtained in the composites [15−17]. In Al−K_2TiF_6−KBF_4 system, some chemical reactions take place in the molten aluminum liquid according to XRD results and thermodynamics calculation results. The formation of the in-situ TiB_2 phases in our experiments is described by the following reactions:

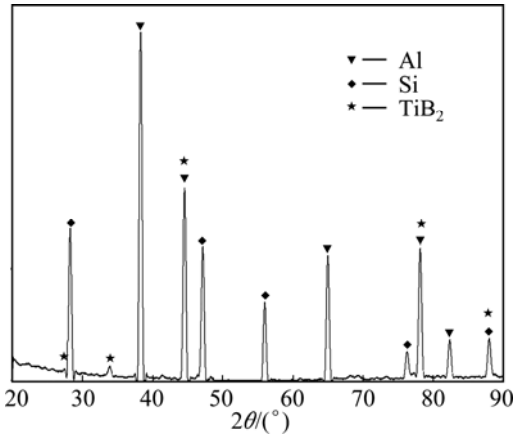

Fig. 2 XRD pattern of prepared composites

$$3K_2TiF_6+13Al=3Al_3Ti+3KAlF_4+K_3AlF_6 \quad (1)$$

$$2KBF_4+3Al=AlB_2+2KAlF_4 \quad (2)$$

$$Al_3Ti+AlB_2=TiB_2+4Al \quad (3)$$

It is suggested that K_2TiF_6 and KBF_4 can react with Al to form TiB_2 phase:

$$6KBF_4+3K_2TiF_6+10Al=9KAlF_4+K_3AlF_6+3TiB_2 \quad (4)$$

$KAlF_4$ and K_3AlF_6 gas ran partly out of the aluminum melt and the residual was degassed by degasifying agent.

3.2 Effects of high-energy ultrasonic field on microstructures of composites

Figure 3 shows the SEM image and energy dispersive spectrum (EDS) of the TiB_2/Al−30Si composites prepared under high-energy ultrasonic field. As shown in Fig. 3(a), the in-situ TiB_2 reinforced particles are uniformly distributed and dispersed in aluminum matrix. The morphology of the in-situ particles is presented in circle-shape or quadrangle-shape with a size of 0.1−1.5 μm. Primary silicon particles are presented in quadrangle-shape with a size of 10 μm. The interfaces between the in-situ TiB_2 particles and aluminum matrix are neat. Figures 3(b) and (c) show the EDS analysis for regions *A* and *B* in Fig. 3(a), respectively. These EDS results further confirm that TiB_2 reinforced phases are formed via in-situ melt reactions from Al−K_2TiF_6−KBF_4 system.

Figure 4 shows SEM images of the TiB_2/Al−30Si composites prepared without and with high-energy ultrasonic field in Al−K_2TiF_6−KBF_4 system. As shown in Fig. 4(a), the morphology of the in-situ TiB_2 particles without the field is not distinct and the particle volume fraction is small. In contrast, the in-situ TiB_2 particles with high-energy ultrasonic field (Fig. 4(b)) are clearly observed and the particle volume fraction is considerably larger (Fig. 4(a)). These results indicate that the melt

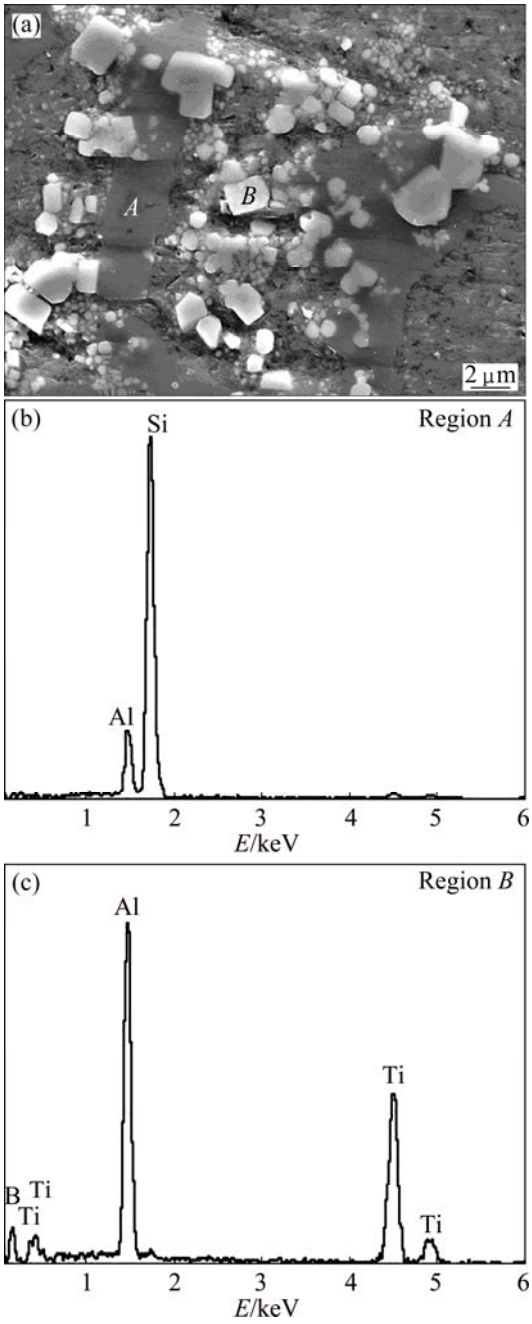

Fig. 3 SEM image (a) and EDS analysis (b, c) of TiB_2/Al−30Si composites prepared under high-energy ultrasonic field

reactions under high-energy ultrasonic field have thoroughly completed while the melt reaction without the field are probably in a transition stage.

Figure 5 shows optical micrographs of the composites prepared without and with high-energy ultrasonic field in Al−K_2TiF_6−KBF_4 system. In order to observe the morphology of the primary silicon, the OM graphs shown in Fig. 5 are in black-white style pattern. Without high-energy ultrasonic field, the morphology of the primary silicon is presented in large snowflake-shape; while with high-energy ultrasonic field, the morphology of the primary silicon is in mass-shape with sizes of

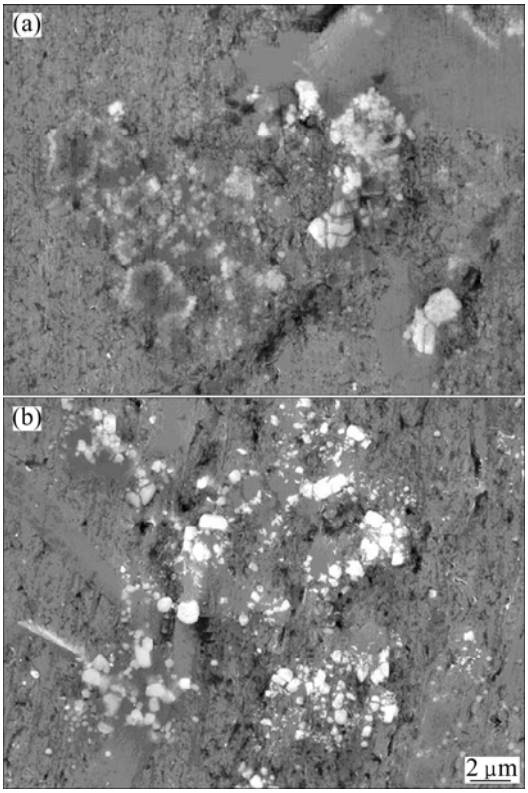

Fig. 4 SEM images of TiB_2/Al−30Si composites prepared in Al−K_2TiF_6−KBF_4 system: (a) Without high-energy ultrasonic field; (b) With high-energy ultrasonic field

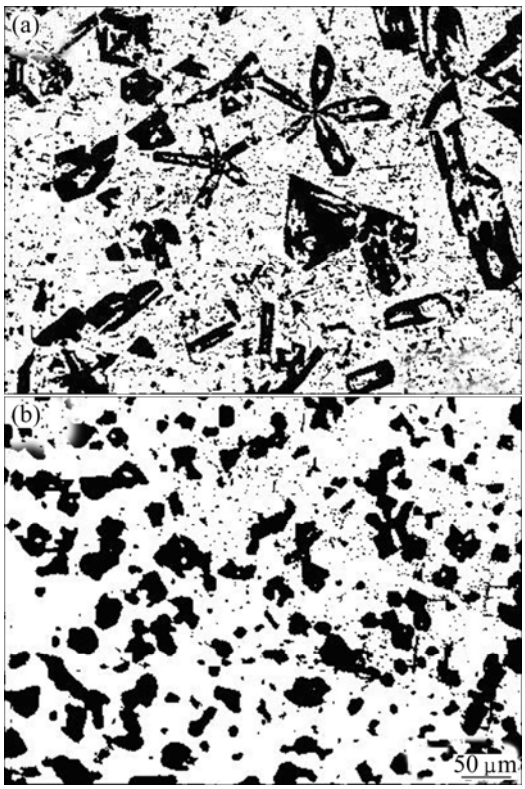

Fig. 5 Optical micrographs of composites fabricated without high-energy ultrasonic field (a) and with high-energy ultrasonic field (b)

10−20 μm. The variations of the morphology of the primary silicon contribute to the wear properties of the prepared composites that will be investigated below.

The effects of ultrasonic power on the optical micrographs of the prepared composites are shown in Fig. 6. It can be clearly seen that the primary silicon is refined and the morphology is optimized with the high energy ultrasonic power increasing from 0 to 1.2 kW. As the high-energy ultrasonic power increases, the acoustic streaming and cavitation effects are intensified. So, the primary silicon is easily broken up, blunted and moved in the stickiness aluminum melt. As a result, the size of the primary silicon becomes small and the ball-shaped silicon is obtained. The mechanism of the high-energy ultrasonic field on the size and morphology of the primary silicon can be interpreted as follows [17].

Firstly, the primary silicon is not an ideal single crystal. Some defects such as pore cave, twin, dislocation, secondary grain boundaries and weak bonding zones exist within primary silicon. Under the acoustic streaming and cavitation effects, the primary silicon is easily broken down in the defect position especially when the primary silicon with large size in length is burst and collided with other primary silicon. The collision force can make the primary silicon broken down along the weak bonding zone. These contribute to the size of the primary silicon decreasing and the morphology blunting.

Secondly, the growth of primary silicon shows obvious anisotropy because of its small facet. As the melt temperature decreases, the preferential growth makes the primary silicon longer in size. In other words, this preferential growth weakens the spherical ability of the primary silicon. However, with the help of the streaming and cavitation effects, the anisotropic growth of the primary silicon is impeded or abated. Furthermore, large amount of mechanical twins can be generated along all directions of primary silicon. These contribute to the flank deposition and growth along the directions for the silicon atom in aluminum melt, and the thickness of the primary silicon is increased. Thus, the preferential growth of the primary silicon is reduced and the spherical ability is increased. As a result, the size and the morphology of the primary silicon are optimized as the streaming and cavitation effects are strengthened with increasing the high energy ultrasonic power.

Thirdly, the curvature of primary silicon's surface increases with increasing the high-energy ultrasonic power. As usual, the larger the curvature of primary silicon's surface is, the higher the content of the balance solute element is. It is suggested that the content of the balance solute element at the interface between primary silicon and aluminum liquid also increases as the curvature increases due to the high-energy ultrasonic

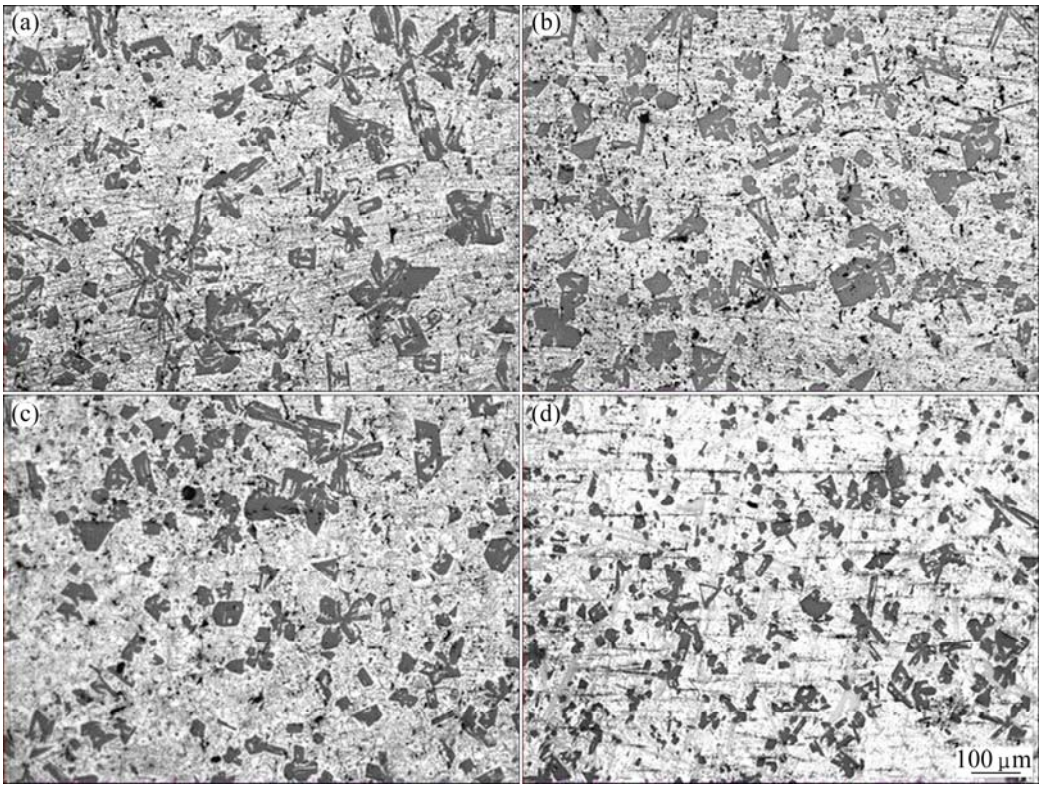

Fig. 6 Effect of ultrasonic field power on size and morphology of primary silicon: (a) 0; (b) 0.6 kW; (c) 0.8 kW; (d) 1.2 kW

field. According to the crystal growth theory, the solute elements tend to diffuse from the large curvature regions to the little ones, which is a spontaneous process from high energy to low one. Therefore, the sharp wedge angle spheroidizing for primary silicon is achieved during this process due to the high-energy ultrasonic field.

3.3 Hardness of composites

The hardness properties of the Al−30Si matrix alloy and the TiB_2/Al−30Si composites fabricated without and with high-energy ultrasonic field are shown in Fig. 7. It indicates that the hardness values of the Al−30Si matrix alloy and the prepared composites obviously increase with increasing the ultrasonic power. At a given ultrasonic power, the hardness value of TiB_2/Al−30Si composites is far higher than that of the Al−30Si matrix alloy. In particular, the maximum hardness value of the in-situ composites is about 1.3 times as high as that of the Al−30Si alloy when the ultrasonic power is 1.2 kW, reaching 412 MPa. It is reasonable to believe that such hardness increase is related to both the refinement of the in-situ TiB_2 particles (Fig. 3(a) and Fig. 4(b)) and the dispersion of the primary Si particles (Fig. 5(b) and Fig. 6(d)) due to the high-energy ultrasonic field.

3.4 Wear properties of composites

Figure 8 shows the variation in mass loss of the

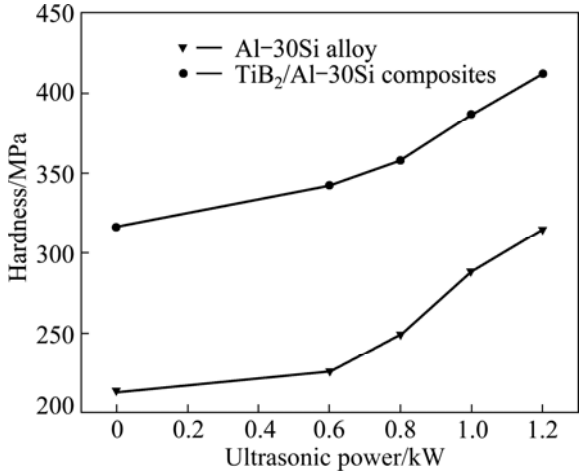

Fig. 7 Hardness of Al−30Si alloy and TiB_2/Al−30Si composites

composites fabricated without and with high-energy ultrasonic field from Al−K_2TiF_6−KBF_4 system. The dry sliding wear parameters are as follows: sliding velocity 0.42 m/s, diameter of the wear track 23 mm, wear time 120 min and different applied loads. As shown in Fig. 8, the wear mass loss values of the composites fabricated with high-energy ultrasonic field are greatly lower than that of the composites fabricated without high-energy ultrasonic field at the same load. For example, as the load is 140 N, the wear mass loss (3.873 mg) of the composites fabricated with high-energy ultrasonic field

is only about 52% of that (7.386 mg) without high-energy ultrasonic field. In addition, with the load increasing from 60 to 140 N, the wear curve of the composites fabricated with high-energy ultrasonic field is flatter than that of the composites without high-energy ultrasonic field. The wear mass loss values only increase from 3.081 to 3.873 mg as the load increases from 60 to 140 N in the case of high-energy ultrasonic field. These results indicate that the wear resistance of the composite fabricated with high-energy ultrasonic field is obviously improved and the wear resistance is insensitive to the amount of applied loads. Obviously, this improved wear resistance is also attributed to the changes of the size and morphology of the in-situ TiB_2 and primary silicon after using the high-energy ultrasonic field.

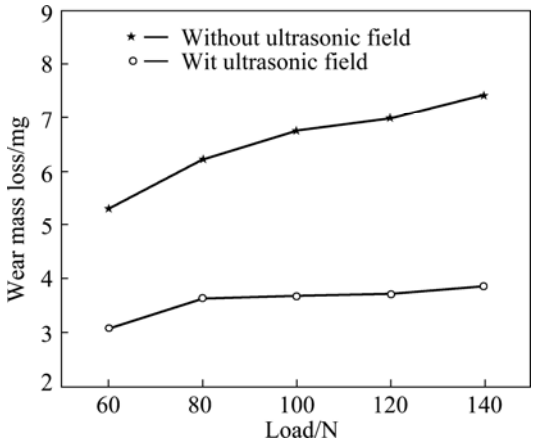

Fig. 8 Mass loss of TiB_2/Al−30Si composites fabricated without and with ultrasonic field

3.5 Worn surface of composites

The micrographs of the worn surface of the composites fabricated without and with high-energy ultrasonic field are shown in Fig. 9. The results reveal that both the worn surfaces of the composites fabricated with and without high-energy ultrasonic field show typical abrasive wear feature (Figs. 9(a) and (b)). The wear path is not homogeneous and a non-uniform wear is noticeable, showing wear outstanding zones and areas with grooves along the sliding direction and plastic deformation after a sliding time of 120 min. Grooves are formed by the reinforcing materials, which include the in-situ TiB_2 particles and the primary silicon particles. The wear inactivation is mainly caused by the two particles above. On these surfaces, fractured appearance areas are observed (Fig. 9). It can be seen that the layer of material has been removed as debris from the surface and the debris is in the form of thin sheets.

4 Conclusions

1) TiB_2/Al−30Si composites were fabricated via in-situ melt reactions under high-energy ultrasonic field. With the assistance of high-energy ultrasonic field, the in-situ TiB_2 reinforced particles are uniformly distributed and dispersed in the aluminum matrix. The morphology of the TiB_2 particles is presented in circle-shape or quadrangle-shape and the size of them is 0.1−1.5 μm. Meanwhile, the size and the morphology of the primary silicon are also optimized using high-energy ultrasonic field. The primary silicon particles are presented in quadrangle-shape and the average size of these particles is about 10 μm.

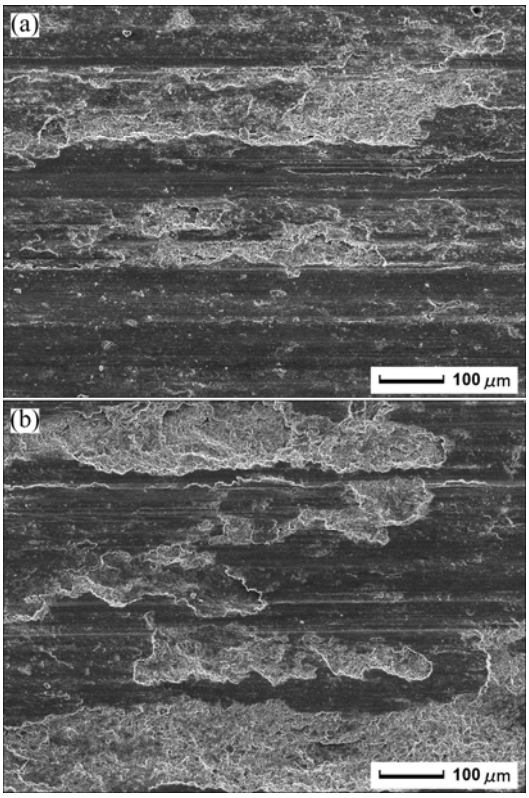

Fig. 9 Micrographs of worn surface of composites fabricated in Al−K_2TiF_6−KBF_4 system: (a) Without high- energy ultrasonic field; (b) With high-energy ultrasonic field

2) The hardness values of both Al−30Si matrix alloy and the prepared composites are significantly increase with increasing high-energy ultrasonic power. In particular, the maximum hardness value of the in-situ composites is about 1.3 times as high as that of the Al−30Si matrix alloy as the ultrasonic power is 1.2 kW, reaching 412 MPa.

3) The wear resistance of the composite prepared under high-energy ultrasonic field is obviously improved and the wear resistance is insensitive to the amount of applied loads. The worn surface of the composites shows typical abrasive wear feature. As the load is 140 N, the wear mass loss of the composites fabricated under high-energy ultrasonic field is only about 52% of that of the composites without high-energy ultrasonic field.

References

[1] SHANKAR S, RIDDLE Y W, MAKHLOUF M M. Nucleation mechanism of the eutectic phases in aluminum–silicon hypoeutectic alloys [J]. Acta Mater, 2004, 52(15): 4447−4460.

[2] IBRAHIM M F, SAMUEL A M, AL-AHMARI A M A, SAMUEL F H. Impact toughness and fractography of Al−Si−Cu−Mg base alloys [J]. Mater Des, 2011, 32(7): 3900−3910.

[3] JELINEK B, GROH S, HORSTEMEYER M F, HOUZE J, KIM S G, WAGNER G J, MOITRA A, BASKES M I. Modified embedded atom method potential for Al, Si, Mg, Cu, and Fe alloys [J]. Phys Rev B, 2012, 85(24): 5102−5113.

[4] JIANG X S, HE G Q, LIU B, FAN S J, ZHU M H. Microstructure-based analysis of fatigue behaviour of Al−Si−Mg alloy [J]. Transactions of Nonferrous Metals Society of China, 2011, 21(3): 443−448.

[5] ZHOU W C, UPRETI S, WHITTINGHAM M S. Electrochemical performance of Al−Si−graphite composite as anode for lithium–ion batteries [J]. Electrochem Commun, 2011, 13(2): 158−161.

[6] LI Y X, LIU J Y, WANG W S, LIU G Q. Microstructures and properties of Al−45%Si alloy prepared by liquid–solid separation process and spray deposition [J]. Transactions of Nonferrous Metals Society of China, 2013, 23(4): 970−976.

[7] FALAK P, NIROUMAND B. Rheocasting of an Al−Si alloy [J]. Scripta Mater, 2005, 53(1): 53−57.

[8] XU C L, WANG H Y, QIU F, YANG Y F, JIANG Q C. Cooling rate and microstructure of rapidly solidified Al−20 wt.%Si alloy [J]. Mater Sci Eng A, 2006, 417(1−2): 275−280.

[9] CUI C, SCHULZ A, SCHIMANSKI K, ZOCH H W. Spray forming of hypereutectic Al−Si alloys [J]. J Mater Process Tech, 2009, 209(11): 5220−5228.

[10] KUCUKOMEROGLU T. Effect of equal-channel angular extrusion on mechanical and wear properties of eutectic Al−12Si alloy [J]. Mater Des, 2010, 31(2): 782−789.

[11] PENG J H, LI W F, HUANG F L, DU J. Effect of rare earth Pr on microstructure and mechanical properties of Al_2O_3−$SiO_{2(sf)}$/Al−Si composites [J]. Transactions of Nonferrous Metals Society of China, 2009, 19(5): 1081−1086.

[12] KÖK M, ÖZDIN K. Wear resistance of aluminium alloy and its composites reinforced by Al_2O_3 particles [J]. J Mater Process Tech, 2007, 183(2−3): 301−309.

[13] SUSLICK K S. The chemical effects of ultrasound [J]. Sci Am, 1989, 2: 80−86.

[14] YANG Y, LAN J, LI X C. Study on bulk aluminum matrix nano-composite fabricated by ultrasonic dispersion of nano-sized SiC particles in molten aluminum alloy [J]. Mater Sci Eng A, 2004, 380(1−2): 378−383.

[15] LAUNDER B E, REECE G J, RODI W. Progress in the development of a Reynolds-stress turbulent closure [J]. J Fluid Mech, 1975, 68(3): 537−566.

[16] FENG Nuo, LI Hua-mao. Phonochemistry and its applications [M]. Hefei: Anhui Science and Technology Press, 1990. (in Chinese)

[17] ARAI N, TAKEDA S, KOHYAMA M. Self-interstitial clustering in crystalline silicon [J]. Phys Rev Lett, 1997, 78(22): 4265−4268.

高能超声场下熔体原位反应制备 TiB_2/Al−30Si 复合材料及其耐磨性能

张松利[1]，董宪伟[2]，赵玉涛[1]，刘满平[1]，陈 刚[1]，张振坤[1]，张宇荧[1]，高雪华[1]

1. 江苏大学 材料科学与工程学院， 镇江 212013；2. 河北联合大学 矿业工程学院，唐山 063009

摘 要：在高能超声场下利用熔体原位反应制备 TiB_2/Al−30Si 复合材料；利用 XRD、SEM 及干磨损试验研究此复合材料的显微组织和磨损性能。结果表明：在高能超声场作用下，原位 TiB_2 颗粒在铝基体中分布均匀，形貌为圆形或四边形，尺寸在 0.1~1.5 μm 之间。初生硅的形貌为四边形，平均尺寸为 10 μm。随着高能超声功率的增加，Al−30Si 基体合金及 TiB_2/Al−30Si 复合材料的硬度明显提高；特别是当超声功率为 1.2 kW 时，复合材料的硬度达到 412 MPa，是基体合金的 1.3 倍。复合材料的磨损性能得到明显提高，载荷的变化对复合材料的磨损量影响不大。

关键词：TiB_2/Al−30Si 复合材料；熔体原位反应；高能超声场；磨损性能

(Edited by Wei-ping CHEN)